Journal of Advanced Research 25 (2020) 205–216

Contents lists available at ScienceDirect

Journal of Advanced Research

journal homepage: www.elsevier.com/locate/jare

Research Article

Numerical evaluation of fractional Tricomi-type model arising from physical problems of gas dynamics

O. Nikan [a], J.A. Tenreiro Machado [b], Z. Avazzadeh [c,d,*], H. Jafari [e]

[a] School of Mathematics, Iran University of Science and Technology, Narmak, Tehran, Iran
[b] Department of Electrical Engineering, ISEP-Institute of Engineering, Polytechnic of Porto, Porto, Portugal
[c] Institute of Research and Development, Duy Tan University, Da Nang 550000, Vietnam
[d] Faculty of Natural Sciences, Duy Tan University, Da Nang 550000, Vietnam
[e] Department of Mathematical Sciences, University of South Africa, UNISA 0003, South Africa

HIGHLIGHTS

- The fractional Tricomi-type model is adopted for describing the anomalous process of nearly sonic speed gas dynamics.
- A new hybrid scheme based LRBF-FD method is formulated to solve the model.
- The LRBF-FD method useful for irregular domains with good accuracy is proposed.
- The stability and convergence of the proposed method are analyzed using the energy method.

GRAPHICAL ABSTRACT

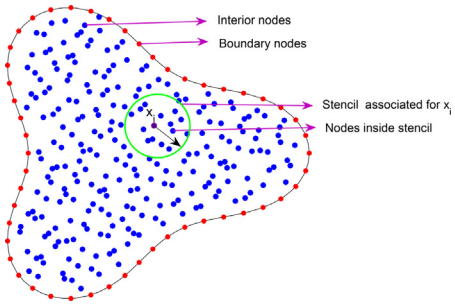

ARTICLE INFO

Article history:
Received 15 April 2020
Revised 3 June 2020
Accepted 21 June 2020
Available online 23 June 2020

Keywords:
Caputo fractional derivative
Time fractional Tricomi-type model
LRBF-FD
Stability analysis

ABSTRACT

This paper deals with approximating the time fractional Tricomi-type model in the sense of the Caputo derivative. The model is often adopted for describing the anomalous process of nearly sonic speed gas dynamics. The temporal semi-discretization is computed via a finite difference algorithm, while the spatial discretization is obtained using the local radial basis function in a finite difference mode. The local collocation method approximates the differential operators using a weighted sum of the function values over a local collection of nodes (named stencil) through a radial basis function expansion. This technique considers merely the discretization nodes of each subdomain around the collocation node. This leads to sparse systems and tackles the ill-conditioning produced of global collocation. The theoretical convergence and stability analyses of the proposed time semi-discrete scheme are proved by means of the discrete energy method. Numerical results confirm the accuracy and efficiency of the new approach.

Introduction

This paper proposes an efficient numerical formulation for solving the time fractional Tricomi-type model (TFTTM), that can be written as

$$\frac{\partial^{\gamma} u(\mathbf{x},t)}{\partial t^{\alpha}} - t^{2\gamma}\Delta u(\mathbf{x},t) = f(\mathbf{x},t), \quad \mathbf{x} = (x,y) \in \Omega \subset \mathbb{R}^2, \quad 0 < t \leqslant T, \tag{1}$$

* Corresponding author.
E-mail addresses: omidnikan77@yahoo.com (O. Nikan), jtm@isep.ipp.pt (J.A.T. Machado), zakiehavazzadeh@duytan.edu.vn (Z. Avazzadeh), jafari.usern@gmail.com (H. Jafari).

https://doi.org/10.1016/j.jare.2020.06.018
2090-1232/

along with the initial and Dirichlet boundary conditions given by

$$u(\mathbf{x},0)=g(\mathbf{x}),\qquad \mathbf{x}\in\bar{\Omega}=\Omega\cup\partial\Omega, \tag{2}$$
$$\frac{\partial u(\mathbf{x},0)}{\partial t}=\psi(\mathbf{x}),\qquad \mathbf{x}\in\bar{\Omega}=\Omega\cup\partial\Omega, \tag{3}$$
$$u(\mathbf{x},t)=h(\mathbf{x},t),\qquad \mathbf{x}\in\partial\Omega,\quad t>0, \tag{4}$$

where T is the final time, Δ denotes the Laplace operator with respect to space variables $\mathbf{x}$, γ is real non-negative number, Ω is a bounded domain in $\mathbb{R}^2$, and $\partial\Omega$ represents the boundary of Ω. The fractional derivative $\partial^\alpha u(\mathbf{x},t)/\partial t^\alpha$ of order $1<\alpha<2$ is defined in the Caputo sense as

$$\frac{\partial^\alpha u(\mathbf{x},t)}{\partial t^\alpha}=\frac{1}{\Gamma(2-\alpha)}\int_0^t\frac{\partial^2 u(\mathbf{x},s)}{\partial s^2}(t-s)^{1-\alpha}\mathrm{d}s,$$

where $\Gamma(\cdot)$ represents the Euler's gamma function [1,2].

During the 20s, Tricomi [3] started the work on the linear partial differential equations of variable type with boundary condition. Later, Frankl [4] showed that the gas flows with nearly sonic speeds could be described by the Tricomi model. For the numerical solution of the TFTTM, we find some works published during the last years. Zhang et al. [5] formulated a local discontinuous Galerkin finite element, Zhang et al. [6] used the finite element scheme and Liu et al. [7] applied the reduced-order finite element technique to approximate the TFTTM. More recently, Dehghan and Abbaszadeh [8] adopted the element-free Galerkin technique and Ghehsareh et al. [9] implemented the local Petrov–Galerkin formulation.

Numerical techniques are extensively applied to approximate partial differential equation (PDE) and we can mention the finite element, finite difference, finite volume, and pseudo-spectral methods. However, usually these techniques are defined on data point meshes meaning that a grid generation is often required, which in turn increases the computation time. Moreover, these schemes have insufficient accuracy over irregular and non-smooth domains because they provide the problem solution only on mesh points. As a result, meshless techniques have been developed to overcome these problems. One important meshless technique is the radial basis function (RBF) method. The RBF is a very efficient instrument for interpolating a scattered set of points and, due to these characteristics, has received attention during last years [10–13]. Indeed, the RBF approximation is a powerful tool that is particularly relevant for high-dimensional problems. Rolland Hardy [14] proposed the RBF technique in 1971 by introducing the multiquadric (MQ) algorithm as a meshless interpolation method using the MQ radial function. Richard Franke [15] popularized this approach in 1982 with a review of the 32 most used interpolation techniques. Franke performed a set of comprehensive tests and concluded that the MQ method had the best overall performance. Furthermore, he advanced that the interpolation matrix related to the MQ radial function has unconditional non-singularity. Later, in 1986, Micchelli [16] proved this using research from the 30s and 40s by Schoenberg. Kansa [17,18] considered the MQ method for approximating elliptic and parabolic PDE. Nonetheless, the well conditioned of the RBF interpolation matrix and good accuracy are not verified simultaneously. This is known as the Uncertainty Principle following the work of Schaback [19]. Fornberg and Larsson [20] implemented this technique to elliptic PDE. The existence, uniqueness, and convergence of the RBF approximation were discussed in detail in several works [21,16,22].

Hereafter, this paper shows that the local RBF is an efficient computational technique to numerically approximate the TFTTM with high accuracy and low computational complexity. Following these ideas, this paper is arranged as follows. Section 2 formulates the temporal discretization via finite difference and discusses its convergence and error analysis. Section 3 applies the local RBF-finite difference (LRBF-FD) for space discretization. Section 4 illustrates the method with three numerical examples that show its efficiency and verify the theoretical analysis. Finally, Section 5 concludes with a summary of the key conclusions.

Temporal discretization

To apply the numerical scheme for the solution of Eq. (1), let $\delta t=T/M, t_k=k\delta t, k=1,\dots,M$, for a positive integer M. Therefore, the time domain $[0,T]$ is covered by temporal discretization points t_k. The following lemmas will be used in the derivation of the time difference scheme [23].

Lemma 1. ([23].) If $1<\alpha<2$ and $g(t)\in C^2[0,T]$, then it follows

$$\int_0^{t_n}g'(s)(t_n-s)^{1-\alpha}\mathrm{d}s=\sum_{k=1}^{n}\frac{g(t_k)-g(t_{k-1})}{\delta t}\int_{t_{k-1}}^{t_k}(t_n-s)^{1-\alpha}\mathrm{d}s+R^n,$$

where

$$|R^n|\leqslant\left(\frac{1}{2(2-\alpha)}+\frac{1}{2}\right)\delta t^{3-\alpha}\max_{0\leqslant t\leqslant t_n}|g''(t)|.$$

Lemma 2. ([23].) Suppose that $1<\alpha<2$ $a_0=\frac{1}{\delta t\Gamma(2-\alpha)}$ and $b_k=\frac{\delta t^{2-\alpha}}{2-\alpha}\left[(k+1)^{2-\alpha}-(k)^{2-\alpha}\right], k=0,1,2,\dots$. Then it follows

$$\begin{aligned}&\left|\tfrac{1}{\Gamma(2-\alpha)}\int_0^{t_n}g'(s)(t_n-s)^{1-\alpha}\mathrm{d}s-a_0\right.\\&\left.\times\left[b_0g(t_n)-\sum_{k=1}^{n-1}(b_{n-k-1}-b_{n-k})g(t_j)-b_{n-1}g(0)\right]\right|\\&\leqslant\tfrac{1}{\Gamma(2-\alpha)}\left(\tfrac{1}{2(2-\alpha)}+\tfrac{1}{2}\right)\delta t^{3-\alpha}\max_{0\leqslant t\leqslant t_n}|g''(t)|.\end{aligned}$$

Lemma 3. ([23].) If $1<\alpha<2$ and $b_k=\frac{\delta t^{2-\alpha}}{2-\alpha}\left[(k+1)^{2-\alpha}-(k)^{2-\alpha}\right]$, $k=0,1,2,\dots$, then it follows

$$b_0>b_1>b_2>\ldots>b_k\to 0, as\ k\to\infty.$$

We introduce the following notation:

$$\delta_t u^{k-\frac{1}{2}}=\frac{u^k-u^{k-1}}{\delta t},\qquad \mu^k=\left(t^k\right)^{2\gamma},\qquad f^{k-\frac{1}{2}}=\frac{f^k+f^{k-1}}{2}. \tag{5}$$

Let us consider

$$v(\mathbf{x},t)=\frac{\partial u(\mathbf{x},t)}{\partial t}, \tag{6}$$

$$\mathscr{V}(\mathbf{x},t_k)=\frac{1}{\Gamma(2-\alpha)}\int_0^t\frac{\partial v(\mathbf{x},s)}{\partial s}(t-s)^{1-\alpha}\mathrm{d}s. \tag{7}$$

From (6) it results that Taylor expansion at $t=t_{k-\frac{1}{2}}$ can be written as:

$$v^{k-\frac{1}{2}}=\delta_t u^{k-\frac{1}{2}}+R_1^{k-\frac{1}{2}}, \tag{8}$$

where

$$\left|R_1^{k-\frac{1}{2}}\right|\leqslant C_1\delta t^2. \tag{9}$$

Based on Lemma 2, we have

$$\mathscr{V}^k=a_0\left[b_0v^n-\sum_{j=1}^{k-1}\left(b_{k-j-1}-b_{k-j}\right)v^j-b_{k-1}v^0\right]+R_2^k$$

and also

$$\mathscr{V}^{k-\frac{1}{2}} = a_0\left[b_0 v^{k-\frac{1}{2}} - \sum_{j=1}^{k-1}\left(b_{k-j-1}-b_{k-j}\right)v^{j-\frac{1}{2}} - b_{k-1}v^0\right] + R_2^{k-\frac{1}{2}},$$

where

$$\left|R_2^{k-\frac{1}{2}}\right| \leqslant C_2\delta t^{3-\alpha}.$$

We define the operator

$$\mathscr{P}\left(v^{k-\frac{1}{2}}, q\right) = a_0\left[b_0 v^{k-\frac{1}{2}} - \sum_{j=1}^{k-1}\left(b_{k-j-1}-b_{k-j}\right)v^{j-\frac{1}{2}} - b_{k-1}q\right]. \tag{10}$$

Using Lemma 2, the expression (10) can be written as

$$\mathscr{V}^{k-\frac{1}{2}} = \frac{\mathscr{V}^{k}+\mathscr{V}^{k-1}}{2} = a_0\mathscr{P}\left(v^{k-\frac{1}{2}}\psi\right) + R_2^{k-\frac{1}{2}}, \tag{11}$$

where $v^0(x) = v(\mathbf{x},0) = \psi(\mathbf{x}) = \psi$. If we substitute (8) into (11), we obtain

$$\mathscr{V}^{k-\frac{1}{2}} = a_0\mathscr{P}\left(\delta_t u^{k-\frac{1}{2}}, \psi\right) + a_0\mathscr{P}\left(R_1^{k-\frac{1}{2}}, 0\right) + R_2^{k-\frac{1}{2}}. \tag{12}$$

Substituting the above result (12) into (1) yields

$$a_0\mathscr{P}\left(\delta_t u^{k-\frac{1}{2}}, \psi\right) = \Delta u^{k-\frac{1}{2}} + f^{k-\frac{1}{2}} + R_2^{k-\frac{1}{2}}, \tag{13}$$

where

$$R^{k-\frac{1}{2}} = -\left\{a_0\mathscr{P}\left(R_1^{k-\frac{1}{2}}, 0\right) + R_2^{k-\frac{1}{2}}\right\}.$$

Based on Lemma 2, 3 and inequalities (9) we can write

$$\begin{aligned}
R^{k-\frac{1}{2}} &\leqslant \left\{a_0\left[b_0 R_1^{k-\frac{1}{2}} + \sum_{j=1}^{k-1}\left(b_{k-j-1}-b_{k-j}\right)v^{j} - b_{k-1}R_1^{k-\frac{1}{2}}\right] + R_2^{k-\frac{1}{2}}\right\}\\
&\leqslant \left\{a_0\left[b_0 C_1\delta t^2 + \sum_{j=1}^{k-1}\left(b_{k-j-1}-b_{k-j}\right)v^{j} - b_{k-1}C_1\delta t^2\right] + C_2\delta t^{3-\alpha}\right\}\\
&= \left\{a_0\left[b_0 C_1\delta t^2 + (b_0-b_{k-1})C_1\delta t^2\right] + C_2\delta t^{3-\alpha}\right\}\\
&\leqslant \left\{a_0\left[2b_0 C_1\delta t^2\right] + C_2\delta t^{3-\alpha}\right\}\\
&= \left\{\tfrac{1}{\delta t\Gamma(2-\alpha)}\left[2\tfrac{\delta t^{2-\alpha}}{2-\alpha}C_1\delta t^2\right] + C_2\delta t^{3-\alpha}\right\}\\
&\leqslant \left(\tfrac{2C_1}{(2-\alpha)\Gamma(2-\alpha)} + C_2\right)\delta t^{3-\alpha}.
\end{aligned}$$

Dropping the error term $R^{k-\frac{1}{2}}$ and approximating the exact value $u^{k-\frac{1}{2}}$ by its numerical approximation $U^{k-\frac{1}{2}}$, leads to the following semi-discrete recursive algorithm:

$$a_0\mathscr{P}\left(\delta_t U^{k-\frac{1}{2}}, \psi\right) = \mu^{k-\frac{1}{2}}\Delta U^{k-\frac{1}{2}} + f^{k-\frac{1}{2}}, \tag{14}$$

or, equivalently, we get

$$\begin{aligned}
&a_0 b_0 U^k - \tfrac{1}{2}\delta t\mu^k\Delta U^k = a_0 b_0 U^{k-1} + \tfrac{1}{2}\delta t\mu^{k-1}\Delta U^{k-1}\\
&+a_0\delta t\sum_{j=1}^{k-1}\left(b_{j-k-1}-b_{j-k}\right)\delta_t U^{j-\frac{1}{2}} + a_0 b_{k-1}\delta t\psi + \tfrac{1}{2}\delta t\left(f^k + f^{k-1}\right).
\end{aligned}$$

Theoretical analysis of the time discretization scheme

We star by defining some functional spaces that will be used in the subsequent discussion. Let us define the functional space endowed with the standard norms and inner products

$$\begin{aligned}
H^1(\Omega) &= \left\{v \in L^2(\Omega), \tfrac{dv}{dx} \in L^2(\Omega)\right\},\\
H_0^1(\Omega) &= \left\{v \in H^1(\Omega), v_{|_{\partial\Omega}} = 0\right\},\\
H^m(\Omega) &= \left\{v \in L^2(\Omega), D^\alpha v \in L^2(\Omega), \text{for all positive integer} |\alpha| \leqslant m\right\},
\end{aligned}$$

where $L^2(\Omega)$ represents the space of measurable functions whose square is Lebesgue integrable in Ω and $\alpha = (\alpha_1, \ldots, \alpha_d)$ denotes a d-tuple of non-negative integer with $|\alpha| = \sum_{i=1}^{d}\alpha_i$. Let us consider

$$D^\alpha v = \frac{\partial^{|\alpha|} v}{\partial x_1^{\alpha}\partial x_2^{\alpha}\ldots\partial x_d^{\alpha}}.$$

The norm $\|v\|_m$ of the space $H^m(\Omega)$ can be written as

$$||v||_{H^m(\Omega)} = \left(\sum_{|\alpha|\leqslant m}||D^\alpha v||^2_{L^2(\Omega)}\right)^{\frac{1}{2}}.$$

Now, let us examine the analysis of stability and the error estimates for the difference algorithm.

Corollary 1. (Poincaré inequality [24]). Suppose that $1 \leqslant p \leqslant \infty$ and that Ω is a bounded open set. Then, there exists a constant $\mathscr{C}_\Omega$ (depending on Ω and p) such that

$$||\boldsymbol{\eta}^{\mathbf{k}}|| \leqslant \mathscr{C}_\Omega||\nabla\boldsymbol{\eta}^{\mathbf{k}}||.$$

Lemma 4. ([23].) For any $G = \{G_1, G_2, \ldots\}$ and q, we have

$$\sum_{j=1}^{M}\mathscr{P}(G_j, q)G_j \geqslant \frac{t_M^{1-\alpha}}{2}\delta t\sum_{j=1}^{M}G_j^2 - \frac{t_M^{2-\alpha}}{2(2-\alpha)}q^2.$$

Lemma 5. ([25].) If x_n is nonnegative sequence and the sequence y_n fulfills

$$\begin{cases} y_0 \leqslant \delta_0,\\ y_n \leqslant \delta_0 + \sum_{k=0}^{n-1} z_k + \sum_{k=0}^{n-1} x_k y_k, \end{cases}$$

then y_n satisfies

$$\begin{cases} y_1 \leqslant \delta_0(1+x_0) + y_0,\\ y_n \leqslant \delta_0 + \prod_{k=0}^{n-2}(1+x_k) + \sum_{k=0}^{n-2} z_k \prod_{s=k+1}^{n-1}(1+x_s) + z_{n-1}, \quad n \geqslant 2. \end{cases}$$

Moreover, if $\delta_0 \geqslant 0$ and $z_n \geqslant 0$ for $n \geqslant 0$, then it holds

$$y_n \leqslant \left(\delta_0 + \sum_{k=0}^{n-1} z_k\right)\exp\left(\sum_{k=0}^{n-1} x_k\right).$$

Making use of these lemmas, we can derive the following result of stability.

Theorem 1. If $U^k \in H_0^1(\Omega)$, then the difference formula (14) is unconditional stable with respect to the H^1-norm.

Proof. The following variational weak formulation will be obtained by multiplying both sides of Eq. (14) by v and integrating over Ω

$$\left\langle a_0\mathscr{P}\left(\delta_t\xi^{k-\frac{1}{2}}, \psi\right), v\right\rangle = \mu^{k-\frac{1}{2}}\left\langle\Delta\xi^{k-\frac{1}{2}}, v\right\rangle, \tag{15}$$

where $\xi^{k-\frac{1}{2}} = U^{k-\frac{1}{2}} - \widetilde{U}^{k-\frac{1}{2}}$ denotes the perturbation at the $(k-\frac{1}{2})$th time level, so that $U^{k-\frac{1}{2}}$ and $\widetilde{U}^{k-\frac{1}{2}}$ are the exact and approximate solutions of Eq. (14), respectively.

Using the divergence theorem

$$\int_\Omega \nabla v\nabla\omega = \int_{\partial\Omega} v\frac{\partial\omega}{\partial\mathbf{n}} - \int_\Omega v\Delta\omega,$$

where

$$\frac{\partial\omega}{\partial\mathbf{n}}=\frac{\partial\omega}{\partial x}n_1+\frac{\partial\omega}{\partial y}n_2$$

is the normal derivative, that is, representing the derivative in the outward normal direction to the boundary $\partial\Omega$, we get

$$a_0\left\{b_0\left\langle\delta_t\xi^{k-\frac{1}{2}},v\right\rangle-\sum_{j=1}^{k-1}\left(b_{k-j-1}-b_{k-j}\right)\left\langle\delta_t\xi^{k-\frac{1}{2}},v\right\rangle\right\}=-\mu^{k-\frac{1}{2}}\left\langle\nabla\xi^{k-\frac{1}{2}},\nabla v\right\rangle. \tag{16}$$

Letting $v=\delta_t\xi^{k-\frac{1}{2}}$ in Eq. (16), we obtain

$$a_0\left\{b_0\left\langle\delta_t\xi^{k-\frac{1}{2}},\delta_t\xi^{k-\frac{1}{2}}\right\rangle-\sum_{j=1}^{k-1}\left(b_{k-j-1}-b_{k-j}\right)\left\langle\delta_t\xi^{j-\frac{1}{2}},\delta_t\xi^{k-\frac{1}{2}}\right\rangle\right\}=-\mu^{k-\frac{1}{2}}\left\langle\nabla\xi^{k-\frac{1}{2}},\nabla\delta_t\xi^{k-\frac{1}{2}}\right\rangle.$$

Summing on $k,k=1,\ldots,M$, and applying Cauchy–Schwarz inequality, we deduce that

$$a_0\sum_{k=1}^{M}\left\{b_0\left\|\delta_t\xi^{k-\frac{1}{2}}\right\|^2-\sum_{j=1}^{k-1}\left(b_{k-j-1}-b_{k-j}\right)\left\|\delta_t\xi^{j-\frac{1}{2}}\right\|\left\|\delta_t\xi^{k-\frac{1}{2}}\right\|\right\}\leqslant\sum_{k=1}^{M}\frac{\mu^{k-\frac{1}{2}}}{2\delta t}\left(\left\|\nabla\xi^{k-1}\right\|^2-\left\|\nabla\xi^{k}\right\|^2\right).$$

Making use of Lemma 4, we can conclude that

$$0\leqslant\frac{t_m^{1-\alpha}}{2\Gamma(2-\alpha)}\sum_{k=1}^{M}\left\|\delta_t\xi^{k-\frac{1}{2}}\right\|^2\leqslant\sum_{k=1}^{M}\frac{\mu^{k-\frac{1}{2}}}{2\delta t}\left(\left\|\nabla\xi^{k-1}\right\|^2-\left\|\nabla\xi^{k}\right\|^2\right)$$

and then

$$\mu^{M-\frac{1}{2}}\|\nabla\xi^{M}\|^2\leqslant\sum_{k=1}^{M}\mu^{k-\frac{1}{2}}\left\|\nabla\xi^{k}\right\|^2\leqslant\sum_{k=1}^{M}\mu^{k-\frac{1}{2}}\left\|\nabla\xi^{k-1}\right\|^2+\mu^{M-\frac{1}{2}}\delta t^{2\alpha+1}\|\nabla\xi^{0}\|^2.$$

If we change the index from M to k, then we arrive at

$$\mu^{k-\frac{1}{2}}\left\|\nabla\xi^{k}\right\|^2\leqslant\sum_{j=0}^{k}\mu^{j-\frac{1}{2}}\left\|\nabla\xi^{j}\right\|^2\leqslant T^{2\alpha}\sum_{j=0}^{k}\left\|\nabla\xi^{j}\right\|^2+\mu^{k-\frac{1}{2}}\delta t^{2\alpha+1}\|\nabla\xi^{0}\|^2.$$

This expression can be rewritten as:

$$\left\|\nabla\xi^{k}\right\|^2\leqslant\sum_{j=0}^{k}\frac{T^{2\alpha}}{\mu^{k-\frac{1}{2}}}\left\|\nabla\xi^{j}\right\|^2+\delta t^{2\alpha+1}\|\nabla\xi^{0}\|^2\leqslant\delta t^{2\alpha+1}\|\xi^{0}\|^2+\sum_{j=0}^{k}T^{2\alpha}\delta t^{-2\alpha}\left\|\nabla\xi^{j}\right\|^2.$$

After applying the discrete Gronwall's lemma to this inequality, it yields

$$\left\|\nabla\xi^{k}\right\|^2\leqslant\left(\delta t^{2\alpha+1}\|\xi^{0}\|^2\right)\sum_{j=0}^{k}\left[1+T^{2\alpha}\delta t^{-2\alpha}\right]=\delta t^{2\alpha}\|\xi^{0}\|^2+T^{2\alpha+1}\|\xi^{0}\|^2\leqslant\left(\delta t^{2\alpha}T^{2\gamma+1}+T^{2\gamma+1}\right)\|\xi^{0}\|^2\leqslant\exp\left(T^{2\gamma+1}\right)\|\xi^{0}\|^2$$

and using the Poincaré inequality, we obtain the desired result

$$\left\|\xi^{k}\right\|\leqslant\sqrt{\exp\left(T^{2\gamma+1}\right)}\|\xi^{0}\|.$$

Hence the proof is complete.

The convergence order of the time-discrete approach is given in the following theorem.

Theorem 2. Let u^k and U^k be the solutions of (13) and (14), respectively, such that both belong to $H_0^1(\Omega)$. Then, the difference formula (14) has convergence order $\mathcal{O}(\delta t^{3-\alpha})$.

Proof. Taking the inner product of Eqs. (13) and (14) with v on the both sides, we obtain their corresponding variational weak form as follows:

$$\left\langle a_0\mathscr{P}\left(\delta_t u^{k-\frac{1}{2}},\psi\right),v\right\rangle=\mu^{k-\frac{1}{2}}\left\langle\Delta u^{k-\frac{1}{2}},v\right\rangle+\left\langle f^{k-\frac{1}{2}},v\right\rangle+\left\langle R^{k-\frac{1}{2}},v\right\rangle \tag{17}$$

and

$$\left\langle a_0\mathscr{P}\left(\delta_t U^{k-\frac{1}{2}},\psi\right),v\right\rangle=\mu^{k-\frac{1}{2}}\left\langle\Delta U^{k-\frac{1}{2}},v\right\rangle+\left\langle f^{k-\frac{1}{2}},v\right\rangle, \tag{18}$$

where $\zeta^{k-\frac{1}{2}}=u^{k-\frac{1}{2}}-U^{k-\frac{1}{2}}$. Subtracting Eq. (17) from Eq. (18) and using the divergence theorem again, we arrive at

$$a_0\left\{b_0\left\langle\delta_t\zeta^{k-\frac{1}{2}},v\right\rangle-\sum_{j=1}^{k-1}\left(b_{k-j-1}-b_{k-j}\right)\left\langle\delta_t\zeta^{k-\frac{1}{2}},v\right\rangle\right\}=-\mu^{k-\frac{1}{2}}\left\langle\nabla\zeta^{k-\frac{1}{2}},\nabla v\right\rangle+\left\langle R^{k-\frac{1}{2}},v\right\rangle. \tag{19}$$

Setting $v=\delta_t\zeta^{k-\frac{1}{2}}$ in Eq. (19) yields

$$a_0\left\{b_0\left\langle\delta_t\zeta^{k-\frac{1}{2}},\delta_t\zeta^{k-\frac{1}{2}}\right\rangle-\sum_{j=1}^{k-1}\left(b_{k-j-1}-b_{k-j}\right)\left\langle\delta_t\zeta^{j-\frac{1}{2}},\delta_t\zeta^{k-\frac{1}{2}}\right\rangle\right\}=-\mu^{k-\frac{1}{2}}\left\langle\nabla\zeta^{k-\frac{1}{2}},\nabla\delta_t\zeta^{k-\frac{1}{2}}\right\rangle+\left\langle R^{k-\frac{1}{2}},\delta_t\zeta^{k-\frac{1}{2}}\right\rangle.$$

Now, we sum from $k=1$ to M to get

$$a_0\sum_{k=1}^{M}\left\{b_0\left\|\delta_t\zeta^{k-\frac{1}{2}}\right\|^2-\sum_{j=1}^{k-1}b_{k-j-1}-b_{k-j})\left\|\delta_t\zeta^{j-\frac{1}{2}}\right\|\left\|\delta_t\zeta^{k-\frac{1}{2}}\right\|\right\}\leqslant-\sum_{k=1}^{M}\frac{\mu^{k-\frac{1}{2}}}{2\delta t}\left(\left\|\nabla\zeta^{k}\right\|^2-\left\|\nabla\zeta^{k-1}\right\|^2\right)+\sum_{k=1}^{M}\left\|R^{k-\frac{1}{2}}\right\|\left\|\delta_t\zeta^{k-\frac{1}{2}}\right\|. \tag{20}$$

In virtue of the Young's inequality, $|\sigma_1\sigma_2|\leqslant\frac{1}{2\vartheta^2}\sigma_1^2+\frac{\vartheta^2}{2}\sigma_2^2$, by choosing $\vartheta=\frac{t_M^{1-\alpha}}{2\Gamma(2-\alpha)}$, we deduce that

$$\sum_{k=1}^{M}\left\|R^{k-\frac{1}{2}}\right\|\left\|\delta_t\zeta^{k-\frac{1}{2}}\right\|\leqslant\frac{\Gamma(2-\alpha)}{t_M^{1-\alpha}}\sum_{k=1}^{M}\left\|R^{k-\frac{1}{2}}\right\|^2+\frac{t_M^{1-\alpha}}{4\Gamma(2-\alpha)}\sum_{k=1}^{M}\left\|\delta_t\zeta^{k-\frac{1}{2}}\right\|^2. \tag{21}$$

Inserting Eq. (21) into Eq. (20), it follows that

$$\frac{t_M^{1-\alpha}}{2\Gamma(2-\alpha)}\sum_{k=1}^{M}\left\|\delta_t\zeta^{k-\frac{1}{2}}\right\|^2\leqslant-\sum_{k=1}^{M}\frac{\mu^{k-\frac{1}{2}}}{2\delta t}\left(\left\|\nabla\zeta^{k}\right\|^2-\left\|\nabla\zeta^{k-1}\right\|^2\right)+\frac{\Gamma(2-\alpha)}{t_M^{1-\alpha}}\sum_{k=1}^{M}\left\|R^{k-\frac{1}{2}}\right\|^2+\frac{t_M^{1-\alpha}}{4\Gamma(2-\alpha)}\sum_{k=1}^{M}\left\|\delta_t\zeta^{k-\frac{1}{2}}\right\|^2. \tag{22}$$

Multiplying Eq. (22) by $2\delta t$, changing M to k, and simplifying results in

$$\left\|\nabla\zeta^{k}\right\|^2\leqslant2\delta tL^2\Gamma(2-\alpha)t_k^{\alpha-1}\sum_{j=1}^{k}\left\|\zeta^{j-\frac{1}{2}}\right\|^2+2\delta t\Gamma(2-\alpha)t_k^{\alpha-1}\sum_{j=1}^{k}\left\|R^{j-\frac{1}{2}}\right\|^2\leqslant2\delta tL^2\Gamma(2-\alpha)t_k^{\alpha-1}\sum_{j=1}^{k}\left\|\zeta^{j-\frac{1}{2}}\right\|^2+2k\delta t\Gamma(2-\alpha)t_k^{\alpha-1}\max_{1\leqslant j\leqslant k}\left\|\zeta^{j-\frac{1}{2}}\right\|^2.$$

Employing a similar technique to the one adopted in the previous theorem yields

$$\left\|\nabla\zeta^{k}\right\|^2\leqslant\delta t^{2\alpha+1}\|\zeta^{0}\|^2+\sum_{j=0}^{k}T^{2\alpha}\delta t^{-2\alpha}\left\|\nabla\zeta^{j}\right\|^2+\sum_{j=1}^{k}2k\delta t\Gamma(2-\alpha)t_k^{\alpha-1}\max_{1\leqslant j\leqslant k}\left\|R^{j-\frac{1}{2}}\right\|^2.$$

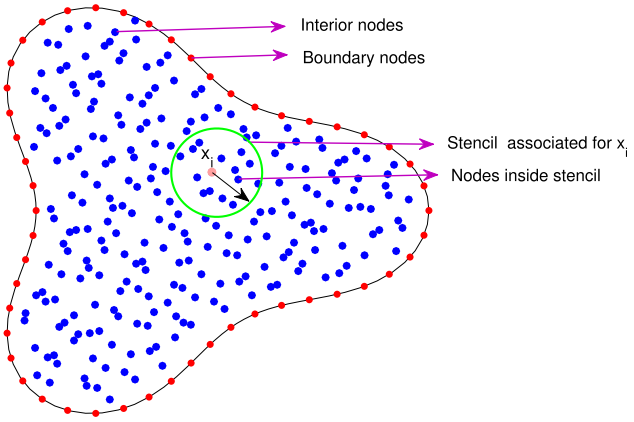

Fig. 1. Schematic diagram of a stencil used for approximating the differential operator on a non-uniform nodes.

Noticing that $\zeta^0 = 0$, we get

$$\left|\left|\nabla\zeta^k\right|\right|^2 \leqslant \sum_{j=0}^{k} T^{2\alpha}\delta t^{-2\alpha}\left|\left|\nabla\zeta^j\right|\right|^2 + 2k\delta t\Gamma(2-\alpha)t_k^{\alpha-1}\max_{1\leqslant j\leqslant k}\left|\left|R^{j-\frac{1}{2}}\right|\right|^2,$$

and applying the Poincaré inequality results in

$$\left|\left|\zeta^k\right|\right|^2 \leqslant \mathscr{C}_\Omega^2\delta t L^2\Gamma(2-\alpha)t_k^{\alpha-1}\sum_{j=1}^{k}\left|\left|\zeta^{j-\frac{1}{2}}\right|\right|^2 + \mathscr{C}_\Omega^2\Gamma(2-\alpha)TC^2\left(\delta t^{3-\alpha}\right)^2. \tag{23}$$

Using the discrete Gronwall inequality, the expression (23) can be rewritten as the following form

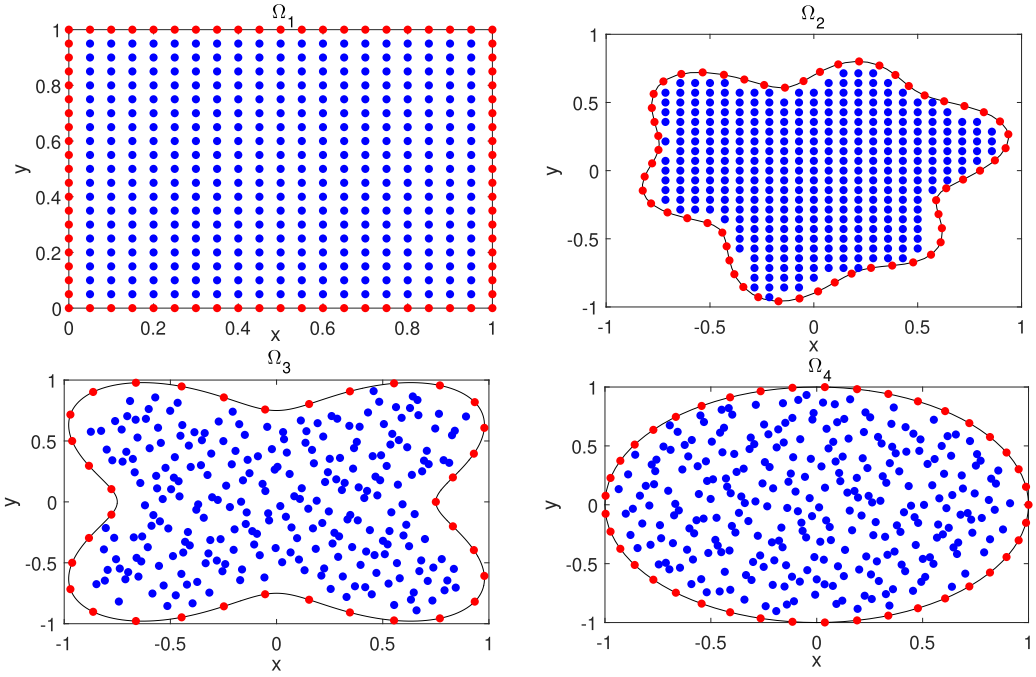

Fig. 2. The computational domains $\{\Omega_1, \Omega_2, \Omega_3, \Omega_4\}$.

Table 1
Numerical errors L_∞ and temporal accuracy $C_{\delta t}$ with $h = 1/10$ and $\alpha = 1.3$ on Ω_1 at $T = 1$.

δt	TPS-RBF $r^4\ln(r)$		MQ-RBF $\sqrt{1+\varepsilon^2r^2}$	
	L_∞	$C_{\delta t}$	L_∞	$C_{\delta t}$
1/10	4.9210e − 03	–	4.0081e − 03	–
1/20	1.7509e − 03	1.4909	1.4613e − 03	1.4557
1/40	5.8335e − 04	1.5857	5.1632e − 04	1.5009
1/80	1.9061e − 04	1.6137	1.6843e − 04	1.6161
1/160	6.1506e − 05	1.6318	5.3772e − 05	1.6472
1/320	1.9502e − 05	1.6571	1.6807e − 05	1.6778
1/640	6.0741e − 06	1.6829	5.1996e − 06	1.6926
1/1280	1.8520e − 06	1.7136	1.5644e − 06	1.7328

Table 2
Numerical errors L_∞ and spatial accuracy C_h on Ω_1.

h	δt	$\alpha = 1.45$		h	δt	$\alpha = 1.65$	
		L_∞	C_h			L_∞	C_h
1/4	1/4	3.3808e − 01	–	1/4	1/4	3.2919e − 01	–
1/8	1/40	1.6495e − 02	4.3573	1/8	1/48	7.9865e − 03	5.3652
1/16	1/400	5.6526e − 04	4.8670	1/16	1/576	4.9705e − 04	4.0061
1/8	1/8	2.6559e − 02	–	1/8	1/8	2.0182e − 02	–
1/16	1/80	1.6845e − 03	3.9788	1/16	1/96	2.1633e − 03	3.2218

Table 3
The absolute errors of the LRBF-FD with $\alpha = 1.8, N = 801$ and $\delta t = 1/100$ at $T = 1$ on Ω_4.

N_l	L_∞	CPU (s)
51	$5.4671e-04$	38.61
71	$5.5065e-04$	45.32
91	$5.6804e-04$	52.17
101	$5.7043e-04$	65.83

Table 4
The obtained condition number and the CPU time for the GRBF and LRBF-FD with $N = 381$ and $\delta t = 1/200$ at $T = 1$.

Domain	Method	CPU (s)	Condition number
Ω_2	GRBF	53.42	$8.6071e+06$
	LRBF-FD	40.21	$3.4948e+02$
Ω_3	GRBF	60.04	$6.7234e+07$
	LRBF-FD	48.51	$5.5923e+02$
Ω_4	GRBF	57.21	$4.6629e+07$
	LRBF-FD	45.34	$5.5911e+02$

$$\begin{aligned}
\left\|\zeta^k\right\|^2 &\leqslant TC^2\mathscr{C}_\Omega^2\Gamma(2-\alpha)\left(\delta t^{3-\alpha}\right)^2 exp\left(\sum_{j=0}^{k-1}\left(\mathscr{C}_\Omega^2 L^2\Gamma(2-\alpha)t_k^{\alpha-1}\right)\right)\\
&\leqslant TC^2\mathscr{C}_\Omega^2\Gamma(2-\alpha)\left(\delta t^{3-\alpha}\right)^2 exp\left(\mathscr{C}_\Omega^2 L^2\Gamma(2-\alpha)k\delta t t_k^{\alpha-1}\right)\\
&= TC^2\mathscr{C}_\Omega^2\Gamma(2-\alpha)\left(\delta t^{3-\alpha}\right)^2 exp\left(\mathscr{C}_\Omega^2 L^2\Gamma(2-\alpha)t_k^{\alpha}\right)\\
&\leqslant TC^2\mathscr{C}_\Omega^2\Gamma(2-\alpha)\left(\delta t^{3-\alpha}\right)^2 exp\left(\mathscr{C}_\Omega^2 L^2\Gamma(2-\alpha)T^2\right)\\
&\leqslant C(T,\alpha,\mathscr{C}_\Omega)\left(\delta t^{3-\alpha}\right)^2.
\end{aligned}$$

As a result, we obtain:

$$\left\|\zeta^k\right\| \leqslant C(T,\alpha,\mathscr{C}_\Omega)\delta t^{3-\alpha}. \tag{24}$$

The proof is completed

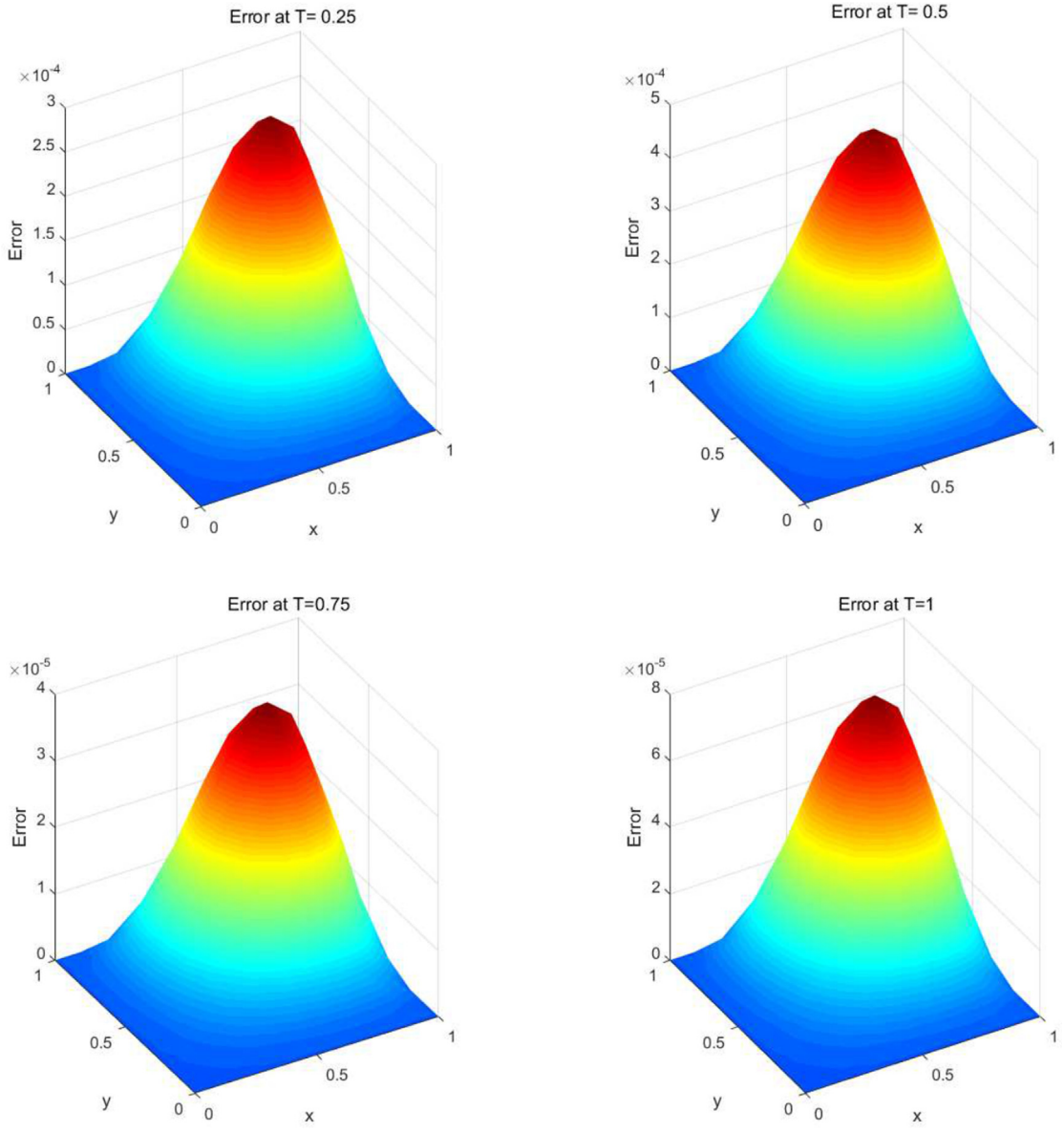

Fig. 3. The absolute error with $\delta t = 1/100, N = 151$ and $\alpha = 1.5$, at $T \in \{0.25, 0.5, 075, 1\}$ on the rectangular domain Ω_1.

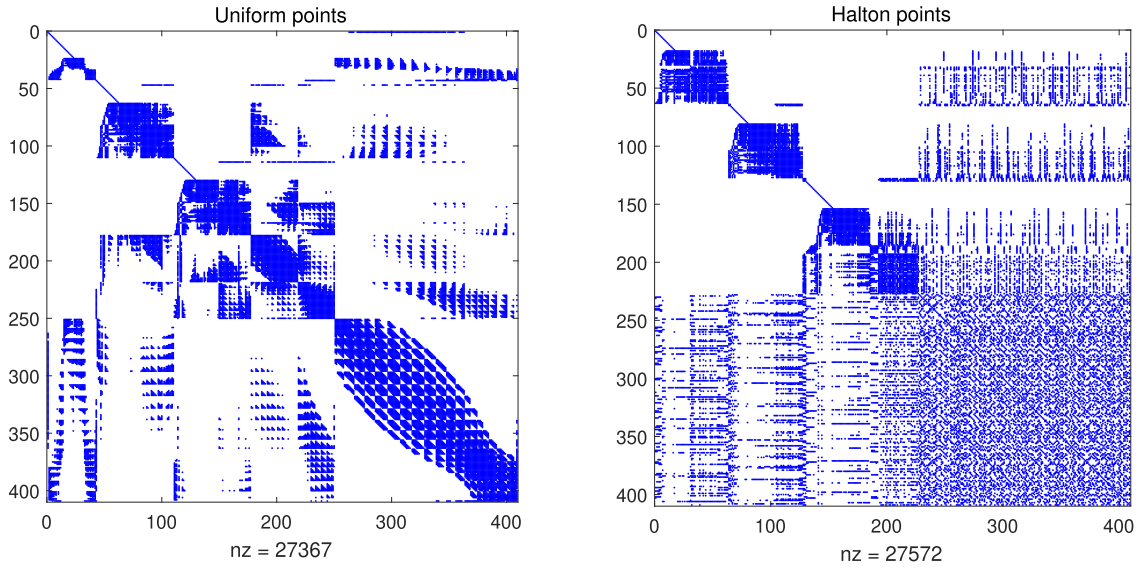

Fig. 4. Sparsity pattern of the coefficient matrix when $N = 400$.

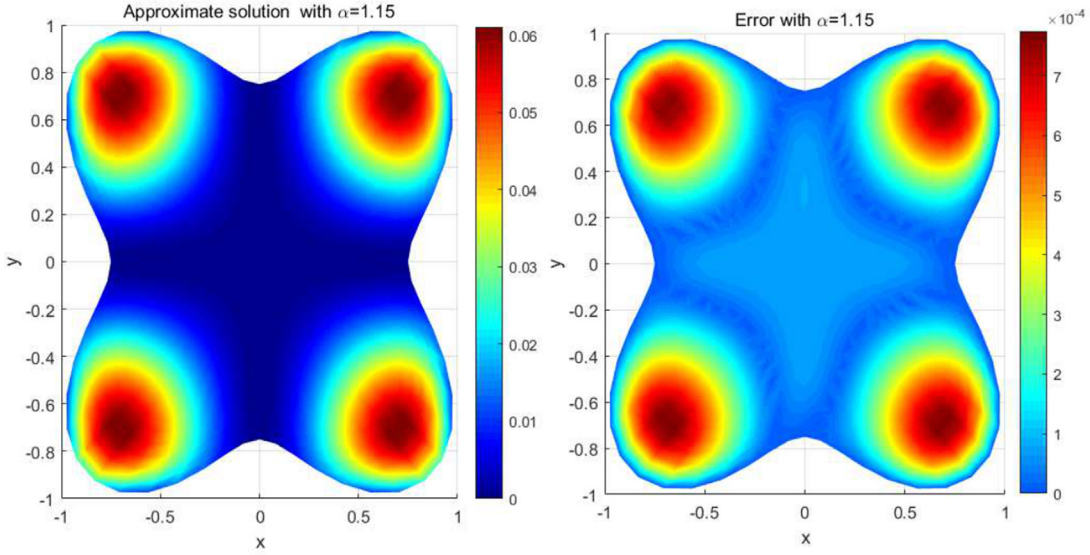

Fig. 5. The approximated solutions and their corresponding absolute errors with $\delta t = 1/100$, at $T = 1$ on Ω_3.

Spatial discretization by the local radial basis function in a finite difference mode

Given a set of distinct nodes $X_C = \{\mathbf{x}_1^c, \ldots, \mathbf{x}_N^c\} \subseteq \mathbb{R}^d$ and the corresponding function values $u(\mathbf{x}_i), i = 1, 2, \ldots, N$, the RBF interpolant is represented in the form

$$u(\mathbf{x}) \simeq S(\mathbf{x}) = \sum_{j=1}^{N} \alpha_j \phi_j(\mathbf{x}, \varepsilon), \tag{25}$$

where $\phi_j(\mathbf{x}, \varepsilon) = \phi\left(\|\mathbf{x} - \mathbf{x}_j^c\|_2, \varepsilon\right), j = 1, \ldots, N$, is a RBF corresponding the j^{th} center with shape parameter ε [26]. The expansion coefficients $\{\alpha_j\}_{j=1}^N$, can be obtained by enforcing the interpolation condition $S(\mathbf{x}_i^c) = u_i^c, i = 1, \ldots, N$, at a set of nodes that usually coincides with the N centers. It is worth to mention that the associated matrix ϕ is a non-singular and invertible for any arbitrarily set of distinct scattered point [16,27].

Kansa [17,18] adopted the linear partial differential operator $\mathscr{L}$ on the interpolation (25) to approximate $\mathscr{L}u$ at the N scatter nodes, namely

$$\mathscr{L}u(\mathbf{x}_i) \simeq \sum_{j=1}^{N} \beta_j \mathscr{L}\phi_j(\mathbf{x}_i, \varepsilon). \tag{26}$$

The relation (26) defines a global RBF (GRBF) approximation, i.e. for approximating $\mathscr{L}$ at reference point $\mathbf{x}_i$, all points in the domain are involved. The GRBF meshless methods have the disadvantage of dense and ill-conditioned interpolation matrices, but, on the other hand, the sparse matrices of these techniques have better condition numbers. Nonetheless, the differentiation matrices associated with local meshless methods, that are used for solving PDE, require the multiplication of the interpolation matrix by its inverse. This results

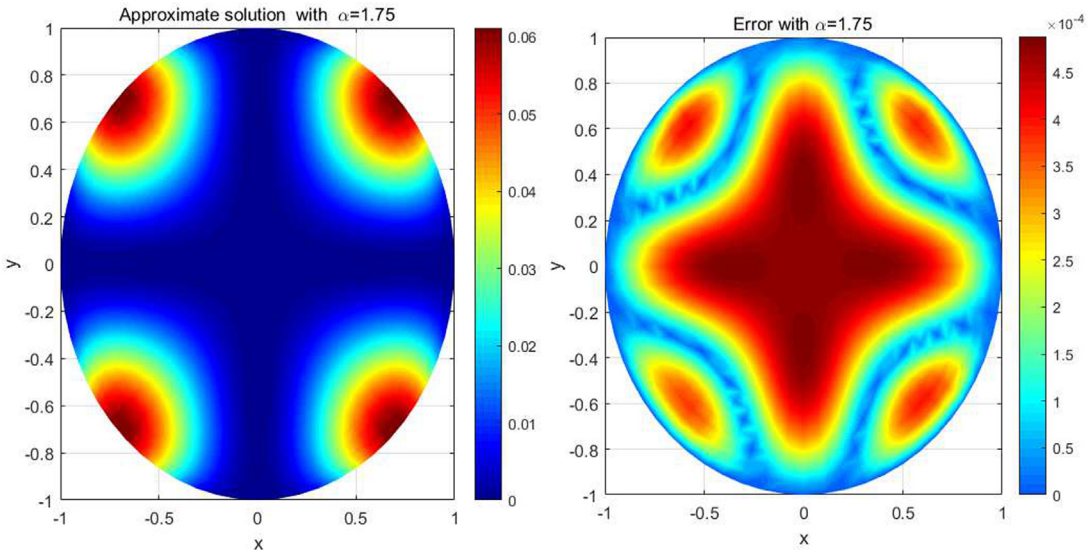

Fig. 6. The approximated solutions and their corresponding absolute errors with $\delta t = 1/100$ and $N = 451$ at $T = 1$ on Ω_4.

Table 5
Numerical errors L_∞ and temporal accuracy $C_{\delta t}$ with $h = 1/10$ and $\alpha = 1.7$ on Ω_1 at $T = 1$.

δt	TPS-RBF $r^4 \ln(r)$		MQ-RBF $\sqrt{1+\varepsilon^2 r^2}$	
	L_∞	$C_{\delta t}$	L_∞	$C_{\delta t}$
1/10	$6.1551e-03$	–	$6.7029e-02$	–
1/20	$3.8996e-03$	1.1460	$3.0289e-03$	1.1460
1/40	$1.7470e-03$	1.1301	$1.3839e-03$	1.1301
1/80	$7.6426e-04$	1.1919	$6.0576e-04$	1.1919
1/160	$3.2383e-04$	1.2021	$2.6329e-04$	1.2021
1/320	$1.3565e-04$	1.2214	$1.1292e-04$	1.2214
1/640	$5.6581e-05$	1.2652	$4.6981e-05$	1.2652
1/1280	$2.3258e-05$	1.3164	$1.8865e-05$	1.3164

Table 6
Numerical errors L_∞ and spatial accuracy C_h on Ω_1.

h	δt	$\alpha = 1.65$		h	δt	$\alpha = 1.45$	
		L_∞	C_h			L_∞	C_h
1/4	1/4	$4.7480e-01$	–	1/4	1/4	$5.0888e-01$	–
1/8	1/40	$9.4222e-03$	5.6551	1/8	1/48	$1.0732e-02$	5.5673
1/16	1/400	$7.7252e-04$	3.6084	1/16	1/576	$9.5886e-04$	3.4845
1/8	1/8	$1.2036e-01$	–	1/8	1/8	$1.3354e-01$	–
1/16	1/80	$4.3565e-03$	4.7880	1/16	1/96	$5.2140e-03$	4.7227

in dense matrices again, and one may use the generalized inverse to solve this limitation. Nonetheless, we must note that the discussion of this subject falls outside the scope of the present work [28–31]. An innovative method named the LRBF-FD has been proposed in [32] to overcome this issue. The new technique was also brought up and examined more extensively in [32–37]. The discretization in LRBF-FD (as a local meshless method) is obtained for a set of local differentiation matrices and adding them up forms a large, sparse system matrix. In order to calculate the differentiation matrix at each point, merely the neighboring points are taken into consideration.

Let us now discuss the proposed method in more detail. For each node $\Xi = \{\mathbf{x}_1, \ldots, \mathbf{x}_N\} \subseteq \mathbb{R}^d$ in space, we consider a subset $\mathscr{S}^I = \left\{\mathbf{x}_1^{(i)}, \ldots, \mathbf{x}_{N_I}^{(i)}\right\} \subseteq \Xi$ consisting of $N_I - 1$ surrounding nodes and $\mathbf{x}_k^{(i)}$ itself, and we define it as a stencil. Fig. 1 illustrates the influence domain of every reference point $\mathbf{x}_i$. In the LRBF-FD, the derivatives of a function in a node requires to be only a list of its nearest stencil. The approximation of an operator $\mathscr{L}$ at the central node $\mathbf{x}_i$ is obtained as a weighted sum of function values of u at the N_I stencil nodes

$$\mathscr{L}u(\mathbf{x}_i) \simeq \sum_{j=1}^{N_I} w_j^{(i)} u\left(\mathbf{x}_j^{(i)}\right). \tag{27}$$

Following [32,33], by using a set of RBF $\{\phi_j(\mathbf{x}, \varepsilon)\}_{j=1}^{N_I}$ centered at $\mathscr{S}^I$ for obtaining the LRBF-FD weights, $\left\{w_j^{(i)}\right\}_{j=1}^{N_I}$, in Eq. (27)

$$\mathscr{L}\phi_k(\mathbf{x}_i, \varepsilon) = \sum_{j=1}^{N_I} w_j^{(i)} \phi_j(\mathbf{x}_k, \varepsilon), \quad k = 1, \ldots, N_I. \tag{28}$$

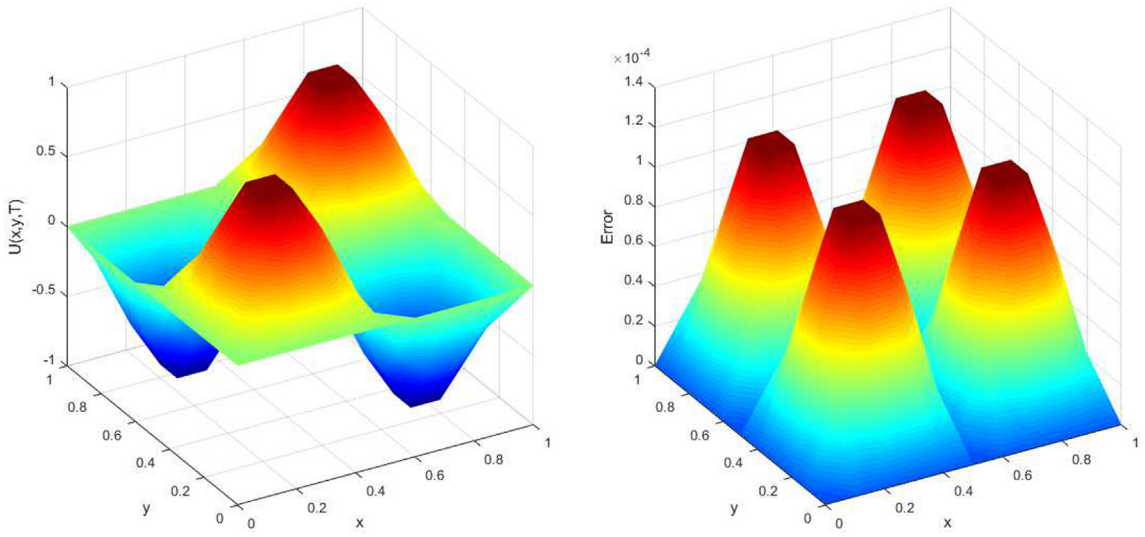

Fig. 7. The approximated solutions and their corresponding absolute errors with $\delta t = 1/100, N = 200$ and $\alpha = 1.5$ at $T = 1$ on the rectangular domain Ω_1.

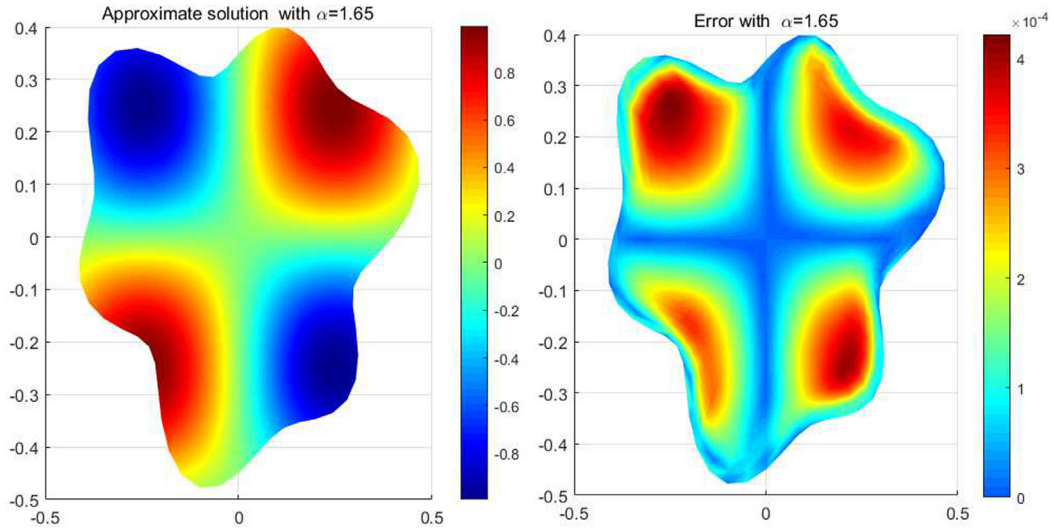

Fig. 8. The approximated solutions and their corresponding absolute errors with $\delta t = 1/100$, at $T = 1$ on Ω_2.

The unknown weights of LRBF-FD can be determined by solving the system of linear equations in the following form:

$$\mathbf{\Phi w}^l = [\mathscr{L}\mathbf{\Phi}]^l, \tag{29}$$

where the coefficient matrix $\mathbf{\Phi}_{N_l \times N_l}$ has entries $\phi_{kj} = \phi_j(\mathbf{x}_k, \varepsilon)$, $\mathbf{w}^l$ represents the $N_l \times 1$ vector of differential weights $\left\{w_j^{(i)}\right\}_{j=1}^{N_l}$, called LRBF-FD weights, and $[\mathscr{L}\mathbf{\Phi}]^l$ is the $N_l \times 1$ vector for the values $\mathscr{L}\phi_k(\mathbf{x}_i, \varepsilon), k = 1, \ldots, N_l$. Due to the nonsingularity of the matrix $\mathbf{\Phi}$ [27], we calculate the weights vector $\mathbf{w}^l$ given by

$$\mathbf{w}^l = \mathbf{\Phi}^{-1}[\mathscr{L}\mathbf{\Phi}]^l. \tag{30}$$

The derivatives are approximated in the LRBF-FD as for the classical FD method. In brief, the derivatives are discretized at any node via the RBF interpolation by means of a small collection of neighboring nodes forming a stencil similar to those obtained with the FD. In the FD the weights $\left\{w_j^{(i)}\right\}_{j=1}^{N_l}$ in the node $\mathbf{x}_i$ are obtained on its stencil values, with the difference that in the LRBF-FD instead of polynomials, the RBF interpolation are used. A fast and effective `kd-tree` algorithm can be used to determine the $N_l - 1$ closest neighboring points in the computation of the differentiation weights for the stencils. We find the `kd-tree` algorithm named `knnsearch` in the statistical toolbox of MATLAB. Additionally, the algorithm by Sarra [38] is used to find the optimal shape parameter.

Results and discussion

This section investigates three problems to highlight the high efficiency of the proposed method and to illustrate the theoretical analysis established in the previous section for different values of h and δt. The rate of convergence in time and space [39] are calculated by using the formulae:

$$C_{\delta t} = \log_2\left(\frac{||L_\infty(2\delta t, h)||}{||L_\infty(\delta t, h)||}\right),$$

$$C_h = \log_2\left(\frac{||L_\infty\left(2^{\frac{4}{3-\alpha}}\delta t, 2h\right)||}{||L_\infty(\delta t, h)||}\right),$$

where $L_\infty = \max_{1 \leqslant j \leqslant N-1} |U(x_j, T) - u(x_j, T)|$. All numerical results are obtained using MATLAB 2016a.

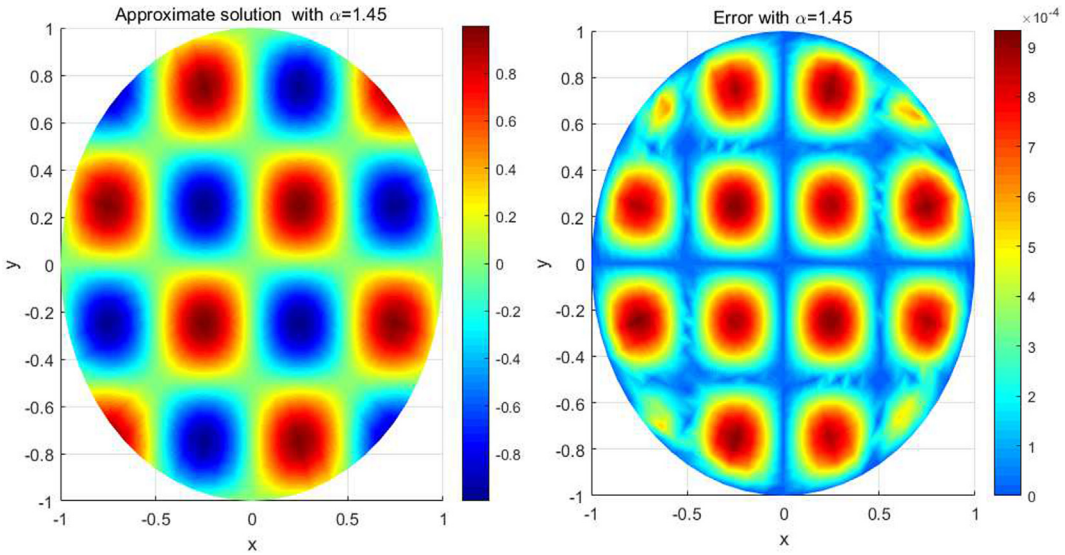

Fig. 9. The approximated solutions and their absolute errors with $\delta t = 1/100$ and $N = 451$ at $T = 1$ on Ω_4.

Table 7
The absolute errors of the LRBF-FD with $N = 401$and $\delta t = 1/80$ at $T = 1$ on Ω_2.

N_I	L_∞	CPU (s)
11	$5.0349e-03$	15.1
15	$5.1589e-03$	17.4
21	$5.1635e-03$	18.3
31	$5.1670e-03$	19.5

Table 8
The obtained condition number and the CPU time for the GRBF and LRBF-FD with $N = 1781$ and $\delta t = 1/1024$ at $T = 1$.

Domain	Method	CPU (s)	Condition number
Ω_2	GRBF	828.69	$3.3064e+10$
	LRBF-FD	502.35	$1.3069e+03$
Ω_3	GRBF	751.14	$3.4601e+10$
	LRBF-FD	463.29	$1.3442e+03$
Ω_4	GRBF	678.47	$4.8933e+10$
	LRBF-FD	352.07	$1.3468e+03$

Fig. 2 shows the computational domains in with two kinds of distribution points that are considered in the follow-up. The domain $\Omega_1 = [0,1]^2$ denotes a rectangular domain with uniformly distributed points. The irregular domain Ω_2 is created using the relation $r(\theta) = 0.8 + 0.1(\sin(6\theta) + \sin(3\theta))$ with uniformly distributed points. The relation $r(\theta) = 1 - \frac{1}{4}\cos(4\theta), 0 \leqslant \theta \leqslant 2\pi$, produces the irregular domain Ω_3 which is covered by Halton distributed points [40]. The domain Ω_4 represents a set of Halton points in the unit circle in $[-1,1]^2$ including Halton non-uniform points.

Example 1. Consider the following TFTTM:

$$\begin{aligned} &\tfrac{\partial^\alpha u(x,y,t)}{\partial t^\alpha} - t^2\Delta u(x,y,t) = \tfrac{6t^2}{\Gamma(4-\alpha)}(x^4-x^2)(y^4-y^2) \\ &-t^4\left((12x^2-2)(y^4-y^2)-(12y^2-2)(x^4-x^2)\right), x,y\in\Omega, 0<t\leqslant T. \end{aligned} \tag{31}$$

The initial and boundary conditions corresponding to this example can be calculated from an exact solution $u(x,y,t) = t^{2+\alpha}(x^4-x^2)(y^4-y^2)$.

The LRBF-FD is applied here with several values for $h, \delta t$ and α, at T on $\Omega_1, \Omega_2, \Omega_3$ and Ω_4. The main results are presented in Tables 1–4 and Figs. 3–6. Tables 1 and 2 report the values achieved for the absolute error and the convergence rates for several values δt and h when $T = 1$ on Ω_1. From Table 1, one can conclude that the obtained computational orders support the theoretical order. Table 3 lists the absolute errors L_∞ of the LRBF-FD for various values of local points N_I. Table 4 exhibits the achieved condition number and CPU time for the GRBF and LRBF-FD on the irregular domains. It is observed that coefficient matrix of LRBF-FD collocation procedure is more well-posed than the coefficient matrix of GRBF method. Fig. 4 shows the sparsity pattern of the matrix associated with the LRBF-FD. Fig. 3 includes the graphs of the absolute

Table 10
Numerical errors E_U^k and temporal accuracy $C_{\delta t}$ with $h = 1/15$ on Ω_1 at $T = 1$.

δt	$\alpha = 1.2$		$\alpha = 1.8$	
	E_U^k	$C_{\delta t}$	E_U^k	$C_{\delta t}$
1/10	$1.0866e-02$	–	$8.3954e-03$	–
1/20	$5.6681e-03$	0.9389	$3.7239e-03$	1.1728
1/40	$2.3676e-03$	1.2594	$1.4702e-03$	1.3408
1/80	$9.5950e-04$	1.3031	$4.9881e-04$	1.5595

Table 9
Comparison of the absolute error in the solution for several values of $h, \delta t$ and α at $T = 1$ on Ω_1.

α	h	δt	LRBF-FD	Ref. [9]	Ref. [7]
1.2	1/10	1/10	$4.4471e-03$	$2.7161e-03$	$8.63934e-02$
	1/20	1/20	$9.0283e-04$	$8.1844e-04$	$2.2133e-02$
	1/40	1/40	$5.6298e-04$	$3.1115e-04$	$5.5200e-03$
1.99	1/10	1/10	$3.6245e-03$	$2.5158e-03$	$8.7656e-02$
	1/20	1/20	$5.6761e-04$	$6.3084e-04$	$2.2912e-02$
	1/40	1/40	$1.9843e-04$	$9.8684e-05$	$5.9500e-03$

Table 11
Numerical errors L_∞ and spatial accuracy C_h with on Ω_1 at $T = 1$.

h	$\alpha = 1.3$		$\alpha = 1.7$	
	L_∞	C_h	L_∞	C_h
2/4, 2/8	2.3540e − 03	–	2.2039e − 03	–
2/8, 2/16	8.7995e − 04	1.1460	6.4571e − 04	1.7711
2/16, 2/32	3.5412e − 04	1.1301	2.3653e − 04	1.4489

errors by choosing $h = 1/10, \delta t = 1/100$ and $\alpha = 1.5$, when $T = 1$ on Ω_1. Fig. 5 depicts the approximate solutions and their absolute errors with $\alpha = 1.15, N = 451$ and $\delta t = 1/100$ when $T = 1$ on Ω_3. Finally, Fig. 6 shows the approximate solutions and their absolute errors with $\alpha = 1.75, N = 353$ and $\delta t = 1/100$, when $T = 1$ on Ω_4.

Example 2. We consider the following TFTTM:

$$\frac{\partial^\alpha u(x,y,t)}{\partial t^\alpha} - t\Delta u(x,y,t) = 2t^2 sin(2\pi x)sin(2\pi y)\left(\frac{t^{-\alpha}}{\Gamma(3-\alpha)} + 4\pi^2 t\right), \quad x,y \in \Omega, \quad 0 < t \leqslant T. \tag{32}$$

The initial and boundary conditions corresponding to this example can be obtained from the exact solution $u(x,y,t) = t^2 \sin(2\pi x)\sin(2\pi y)$.

The LRBF-FD is formulated here for different quantities of $\delta t, h$ and α, at T on $\Omega_1, \Omega_2, \Omega_3$ and Ω_4. The results are illustrated in Tables 5 and 8 and Figs. 7–9. Tables 5 and 6 report the values achieved for the absolute error and the convergence rates for several values δt and h when $T = 1$ on Ω_1. From Table 5, one can conclude that the computational order is in good agreement with the theoretical order. Table 7 illustrates the absolute errors L_∞ of the LRBF-FD for several values of local points N_l. Table 8 reports the obtained condition number and the CPU time for the GRBF and LRBF-FD on the irregular domains. It can be mentioned that coefficient matrix of the LRBF-FD collocation procedure is more smaller than the coefficient matrix of the GRBF. Table 9 compares the absolute errors of the RBF-FD and those from [7,9] with several values of δt and h. Fig. 7 represents the resulting absolute errors by choosing $h = 1/10, \delta t = 1/100$ and $\alpha = 1.5$, when $T = 1$ on Ω_1. Fig. 8 includes the absolute errors achieved with $N = 451, \delta t = 1/100$ for $\alpha = 1.65$, when $T = 1$ on Ω_2. Finally, Fig. 9 displays the approximate solutions and their absolute errors with $\alpha = 1.45, N = 353$ and $\delta t = 1/100$, when $T = 1$ on Ω_4.

Example 3. Lastly, we consider the following TFTTM:

$$\frac{\partial^\alpha u(x,y,t)}{\partial t^\alpha} - t\Delta u(x,y,t) = 0, \quad x,y \in \Omega, \quad 0 < t \leqslant T,$$

with the initial conditions

$$u(x,y,0) = 0, \quad \frac{\partial u(x,y,0)}{\partial t} = 0, \quad x,y \in \Omega$$

and boundary condition

$$u(x,y,t) = t^{2+\alpha}\cos(2\pi x)\cos(2\pi y), \quad x,y \in \partial\Omega.$$

Since the analytical solution of the above problem is unknown, we apply the relation presented by Kamranian et al. [41] for the criterion convergence of the solution:

$$E_U^k = \frac{\|U^{k+1} - U^k\|}{\|U^{k+1}\|}, \tag{33}$$

where the error at δt is evaluated as a difference between the solutions $U_{\delta t}$ and $U_{2\delta t}$ for time steps δt and $2\delta t$ at T given by $E_{\delta t} = \|U_{\delta t} - U_{2\delta t}\|$. The following predictor–corrector procedure and norm are illustrated to obtain the error in spatial variable

$$E_{h_1,h_2} = \|U_{h_1} - U_{h_2}\|, \tag{34}$$

where U_{h_1} and U_{h_2} are the approximate solutions with respect to h_1 and h_2, respectively. The spatial convergence rate can be calculated as:

$$C_h = \log_2\left(\frac{E_{h,h/2}}{E_{h/2,h/4}}\right), \tag{35}$$

where $E_{h,h/2}$ and $E_{h/2,h/4}$ are the absolute error between the solutions with mesh sizes $\{h, h/2\}$ and $\{h/2, h/4\}$, respectively.

We apply the LRBF-FD to obtain the numerical results for several quantities of $\delta t, h$ and α. Table 10 reports the achieved errors and convergence orders with respect to the temporal domain. Table 11 lists the achieved errors and convergence orders with respect to the spatial domain.

Concluding remarks

This paper presented a novel method for finding an approximate solution of the TFTTM. One of the key results that emerges from this work is that the method is robust and has a reliable accuracy even for a complex domain using irregular nodal distributions. It ought to be said here that the irregularly nodal distribution and complex domain lead to considerable difficulties for standard techniques. The proposed algorithm includes two parts, namely, a first one where the problem is discretized based on finite difference scheme in the temporal direction, and a second one where the LRBF-FD is used for the spatial approximation. The stability and convergence of the semi-discrete scheme are rigorously investigated. Numerical results highlight the efficiency of the method.

Declaration of Competing Interest

The authors declare that there is no conflict of interests regarding the publication of this manuscript.

Compliance with Ethics Requirements

This manuscript does not contain any studies with human participants or animals performed by any of the authors.

Acknowledgement

The authors are very grateful to the reviewers for their valuable comments on the manuscript that led to many improvements.

References

[1] Samko SG, Kilbas AA, Marichev OI, et al. Fractional integrals and derivatives. Gordon and Breach Science Publishers, Vol. 1. Switzerland: Yverdon Yverdon-les-Bains; 1993.

[2] Kilbas AA, Srivastava HM, Trujillo JJ. Theory and applications of fractional differential equations, Vol. 204. Elsevier Science Limited; 2006.
[3] Tricomi F. Sulle equazioni lineari alle derivate Parziali di secondo ordine, di tipo misto. Rend Reale Accad Lincei Cl Sci Fis Mat Natur 1923;5(14):134–247.
[4] Frankl F. On the problems of Chaplygin for mixed sub-and supersonic flows. Bull Acad Sci USSR Ser Math 1945;8:195–224.
[5] Zhang X, Liu J, Wen J, Tang B, He Y. Analysis for one-dimensional time-fractional Tricomi-type equations by LDG methods. Numer Algor 2013;63 (1):143–64.
[6] Zhang X, Huang P, Feng X, Wei L. Finite element method for two-dimensional time-fractional Tricomi-type equations. Numer Methods Partial Diff Eqs 2013;29(4):1081–96.
[7] Liu J, Li H, Liu Y, Fang Z. Reduced-order finite element method based on POD for fractional Tricomi-type equation. Appl Math Mech 2016;37(5):647–58.
[8] Dehghan M, Abbaszadeh M. Element free Galerkin approach based on the reproducing kernel particle method for solving 2D fractional Tricomi-type equation with Robin boundary condition. Comput Math Appl 2017;73 (6):1270–85.
[9] Ghehsareh HR, Raei M, Zaghian A. Application of meshless local Petrov-Galerkin technique to simulate two-dimensional time-fractional Tricomi-type problem. J Brazil Soc Mech Sci Eng 2019;41(6):252.
[10] Hosseininia M, Heydari M. Meshfree moving least squares method for nonlinear variable-order time fractional 2D telegraph equation involving Mittag-Leffler non-singular kernel. Chaos, Solitons & Fractals 2019;127:389–99.
[11] Shekari Y, Tayebi A, Heydari MH. A meshfree approach for solving 2D variable-order fractional nonlinear diffusion-wave equation. Comput Methods Appl Mech Eng 2019;350:154–68.
[12] Hosseininia M, Heydari M, Avazzadeh Z. Numerical study of the variable-order fractional version of the nonlinear fourth-order 2D diffusion-wave equation via 2D Chebyshev wavelets. Eng Comput 2020:1–10.
[13] Hosseininia M, Heydari M, Rouzegar J, Cattani C. A meshless method to solve nonlinear variable-order time fractional 2D reaction–diffusion equation involving Mittag-Leffler kernel. Eng Comput 2019:1–13.
[14] Hardy RL. Multiquadric equations of topography and other irregular surfaces. J Geophys Res 1971;76(8):1905–15.
[15] Franke R. Scattered data interpolation: tests of some methods. Math Comput 1982;38(157):181–200.
[16] Micchelli CA. Interpolation of scattered data: distance matrices and conditionally positive definite functions. In: Approximation theory and spline functions. Springer; 1984. p. 143–5.
[17] Kansa EJ. Multiquadrics-a scattered data approximation scheme with applications to computational fluid-dynamics-I surface approximations and partial derivative estimates. Comput Math Appl 1990;19(8–9):127–45.
[18] Kansa EJ. Multiquadrics-a scattered data approximation scheme with applications to computational fluid-dynamics-II solutions to parabolic, hyperbolic and elliptic partial differential equations. Comput Math Appl 1990;19(8–9):147–61.
[19] Schaback R. Error estimates and condition numbers for radial basis function interpolation. Adv Comput Math 1995;3(3):251–64.
[20] Larsson E, Fornberg B. A numerical study of some radial basis function based solution methods for elliptic PDEs. Comput Math Appl 2003;46(5–6):891–902.
[21] Franke C, Schaback R. Convergence order estimates of meshless collocation methods using radial basis functions. Adv Comput Math 1998;8(4):381–99.
[22] Madych W, Nelson S. Multivariate interpolation and conditionally positive definite functions. ii. Math Comput 1990;54(189):211–30.
[23] Sun Z-Z, Wu X. A fully discrete difference scheme for a diffusion-wave system. Appl Numer Math 2006;56(2):193–209.
[24] Brezis H. Functional analysis, Sobolev spaces and partial differential equations. Springer Science & Business Media; 2010.
[25] Der van Houwen P, Quarteroni A, Valli A. Numerical approximation of partial differential equations. Berlin etc., springer-verlag 1994. xvi, 543 pp., dm 128, 00. isbn 3-540-57111-6 (springer series in computational mathematics 23), Zeitschrift Angewandte Mathematik und Mechanik 1995;75: 550–550.
[26] Rasoulizadeh MN, Rashidinia J. Numerical solution for the Kawahara equation using local RBF-FD meshless method. J King Saud Univ-Sci 2020;32 (4):2277–83.
[27] Wendland H. Scattered data approximation, Vol. 17. Cambridge University Press; 2004.
[28] Oanh DT, Davydov O, Phu HX. Adaptive RBF-FD method for elliptic problems with point singularities in 2D. Appl Math Comput 2017;313:474–97.
[29] Bayona V, Flyer N, Fornberg B. On the role of polynomials in RBF-FD approximations: III. Behavior near domain boundaries. J Comput Phys 2019;380:378–99.
[30] Dehghan M, Abbaszadeh M. The use of proper orthogonal decomposition (POD) meshless RBF-FD technique to simulate the shallow water equations. J Comput Phys 2017;351:478–510.
[31] Dehghan M, Mohammadi V. A numerical scheme based on radial basis function finite difference (RBF-FD) technique for solving the high-dimensional nonlinear Schrödinger equations using an explicit time discretization: Runge-Kutta method. Comput Phys Commun 2017;217:23–34.
[32] Tolstykh A, Shirobokov D. On using radial basis functions in a "finite difference mode" with applications to elasticity problems. Comput Mech 2003;33 (1):68–79.
[33] Wright GB, Fornberg B. Scattered node compact finite difference-type formulas generated from radial basis functions. J Comput Phys 2006;212(1):99–123.
[34] Nikan O, Machado JT, Golbabai A, Nikazad T. Numerical approach for modeling fractal mobile/immobile transport model in porous and fractured media. Int Commun Heat Mass Transf 2020;111:104443.
[35] Nikan O, Golbabai A, Machado JT, Nikazad T. Numerical approximation of the time fractional cable equation arising in neuronal dynamics. Eng Comput 2020:1–19. doi: https://doi.org/10.1007/s00366-020-01033-8.
[36] Nikan O, Golbabai A, Machado JT, Nikazad T. Numerical solution of the fractional Rayleigh-Stokes model arising in a heated generalized second-grade fluid. Eng Comput 2020:1–14. doi: https://doi.org/10.1007/s00366-019-00913-y.
[37] Nikan O, Machado JT, Golbabai A, Nikazad T. Numerical investigation of the nonlinear modified anomalous diffusion process. Nonlinear Dynam 2019;97 (4):2757–75.
[38] Sarra SA. A local radial basis function method for advection–diffusion–reaction equations on complexly shaped domains. Appl Math Comput 2012;218 (19):9853–65.
[39] Cui M. Compact finite difference schemes for the time fractional diffusion equation with nonlocal boundary conditions. Comput Appl Math 2018;37 (3):3906–26.
[40] Fasshauer GE. Meshfree Approximation Methods with Matlab: (With CD-ROM), Vol. 6. World Scientific Publishing Company; 2007.
[41] Kamranian M, Dehghan M. The finite point method for reaction-diffusion systems in developmental biology. CMES Comput Model Eng Sci 2011;82 (1):1–27.